Generation of Nondegenerate Narrow-Band Photon Pairs for a Hybrid Quantum Network

Jian Wang, Peng-YinJie Lv, Jin-Ming Cui, Bi-Heng Liu, Jian-Shun Tang, Yun-Feng Huang,* Chuan-Feng Li,† and Guang-Can Guo

Key Laboratory of Quantum Information, University of Science and Technology of China, CAS, Hefei 230026, People's Republic of China and Synergetic Innovation Centre in Quantum Information and Quantum Physics, University of Science and Technology of China, Hefei, Anhui 230026, China

(Received 10 August 2015; revised manuscript received 7 December 2015; published 29 December 2015)

In a hybrid quantum network, the linking of two types of quantum nodes through photonic channels requires excellent matching of the central frequency and bandwidth between both nodes and their interfacing photons. However, preexisting photon sources cannot fulfill this requirement. Using a novel conjoined double-cavity strategy, we report the generation of nondegenerate narrow-band photon pairs by cavity-enhanced spontaneous parametric down-conversion. The central frequencies and bandwidths of the signal and idler photons are independently set to match with trapped ions and solid-state quantum memories. With this source we achieve the bandwidths and central wavelengths of 4 MHz at 935 nm and 5 MHz at 880 nm for the signal and idler photons, respectively, with a normalized spectral brightness of 4.9 photon pairs/(s MHz mW). Because of its ability to be independently locked to two different wavelengths, the conjoined double cavity is universally suitable for a hybrid quantum network consisting of various quantum nodes.

DOI: 10.1103/PhysRevApplied.4.064011

I. INTRODUCTION

The realization of quantum networks composed of quantum nodes and quantum channels is of great importance to the distributed quantum computation and quantum communication. The function of the quantum node is the operation and storage of the quantum state, and the function of the quantum channel is the distribution of quantum information [1]. Much experimental progress has been achieved in this aspect for different physical systems, such as atomic ensembles, single atoms, and trapped ions [2–4]. In comparison, hybrid quantum networks consisting of various physical systems [5,6] can combine the different advantages of diverse physical systems. However, the central frequencies of photons for the interfaces linking the nodes built with different physical systems are usually not identical. To solve this problem, previously reported proposals include coherent quantum-frequency conversion [7], tailoring the frequency of one kind of node to be the same as the other [6], or interconnecting the nodes with nondegenerate photon pairs [8].

As an advantage of the hybrid quantum network, different physical systems can be chosen as computing or storing nodes. For the computing nodes, trapped ions can be a suitable candidate because they are one of the most promising physical systems for the realization of quantum computation and simulation [9,10]. The creation of Greenberger-Horne-Zeilinger states in an ion trap has been demonstrated for up to 14 qubits [11], and two-dimensional Ising interactions simulated with hundreds of spins [12] have been reported in the experiment. A quantum network based on trap ions should have the ability to interconvert stationary and flying qubits [13]. Emitted photon-ion entanglement and photon-mediated entanglement have been demonstrated in previous experiments [14,15]. Recently, experimental results have shown that single photons can be absorbed by the trapped single ion [6,16,17]. However, to the best of our knowledge, a customized narrow-band photon-pair source suitable for trapped ions has not been reported. For the storing nodes, a promising candidate is the rare-earth ion-doped crystal system, because it has already shown excellent merit in regard to quantum memory [18,19]. There have been many major advances in the development of rare-earth ion-doped crystal-based quantum memory, including the demonstration of stopped light and image storage up to the regime of one minute [20], and up to 0.999 process fidelity for the storage and retrieval process of a single-photon-level coherent pulse [21]. Moreover, recent progress includes the storage of photonic high-dimensional orbital-angular-momentum entanglement [22], the storage of a telecom-wavelength time-bin entanglement [23], quantum teleportation of the polarization state of a telecom-wavelength photon onto the state of a solid-state quantum memory [24], and the preservation of quantum coherence on an hour-long time scale [25]. In view of these achievements, the realization of photonic channels linking the trapped ions and the rare-earth ion-doped crystals should be useful in a hybrid quantum network.

*hyf@ustc.edu.cn
†cfli@ustc.edu.cn

Compared to photon pairs generated by a cold atomic system [17,26], the cavity-enhanced spontaneous parametric down-conversion (SPDC) process is much more flexible and less complicated in regard to providing photonic channels. Passive filtering with optical etalon is also a direct means used to obtain band-matched narrow-band photon pairs from a single-pass SPDC source [16], but it will tremendously decrease the photon counting rate. During the process of cavity-enhanced SPDC, the down-conversion of photons with the frequency and spatial mode matched to the cavity mode is greatly enhanced, otherwise, it is greatly suppressed [27], resulting in the generation of photon pairs with a flexible bandwidth and a perfect spatial mode. Since the first cavity-enhanced SPDC was demonstrated [27], many experiments have been performed for different purposes [28–33]. Recently, nondegenerate narrow-band photon pairs have been generated through different methods [33–35]. However, the linking of two types of physical systems requires an excellent match of the central frequencies and the bandwidths for each node at the same time. In the experiments [33], the frequency of idler photons can be only certain values determined by the frequency of the signal photons because of the locking system. In the experiments [34,35], the frequencies of two photons change together with the tuning of temperature. Therefore, the requirement cannot be fulfilled in the above experiments.

II. EXPERIMENTAL FRAMEWORK

In this paper, we demonstrate a way to generate nondegenerate narrow-band photon pairs with a conjoined double-cavity (CDC) structure, and the central frequency and bandwidth are well matched to the trapped ion Yb^{+} [6] and the Nd^{3+}-doped solid-state quantum memory [21]. The good match of central frequency is ensured by the fact that the two cavities in the CDC structure are independently locked on the resonance absorption lines of two different types of nodes, and the bandwidth match is ensured by the modified design of two individual cavities. The measured bandwidths of the generated photon pairs is 4 MHz at 935 nm and 5 MHz at 880 nm. To further take advantage of the long coherence time of narrow-band photons, the single-mode output of photons is realized by the temperature-controlled etalon filter.

The experimental setup of our narrow-band photon pair source is shown in Fig. 1. Two semiconductor external-cavity-diode lasers with target wavelengths at 880 nm (Moglabs) and 935 nm (Toptica DL pro) are tuned to the working wavelengths of quantum memory and trapped ion. Two lasers are locked to the same ultrastable Fabry-Pérot cavity with a 1-MHz bandwidth and 1500 finesses (Stable Laser Systems) with the Pound-Drever-Hall scheme, which is not shown here [36]. The 453-nm pump laser is provided by the sum-frequency generation of the two 880-nm and 935-nm lasers for the next-step SPDC process. The sum-frequency-generation process mainly consists of a 1-cm-long periodically poled lithium-niobate waveguide (HCPhotonics Corp). In the cavity-enhanced SPDC process, a 2-cm-long periodically poled KTiOPO4 (PPKTP) crystal is used as the nonlinear crystal. The type-II quasi-phase-matching is fabricated for the polarization of a 453-nm pump laser, parallel with the polarization of 935-nm laser. The calculated theoretical bandwidth of the phase matching is 120 GHz. As shown in Fig. 1, a customized dichroic mirror (DM) is inserted in the optical cavity, which

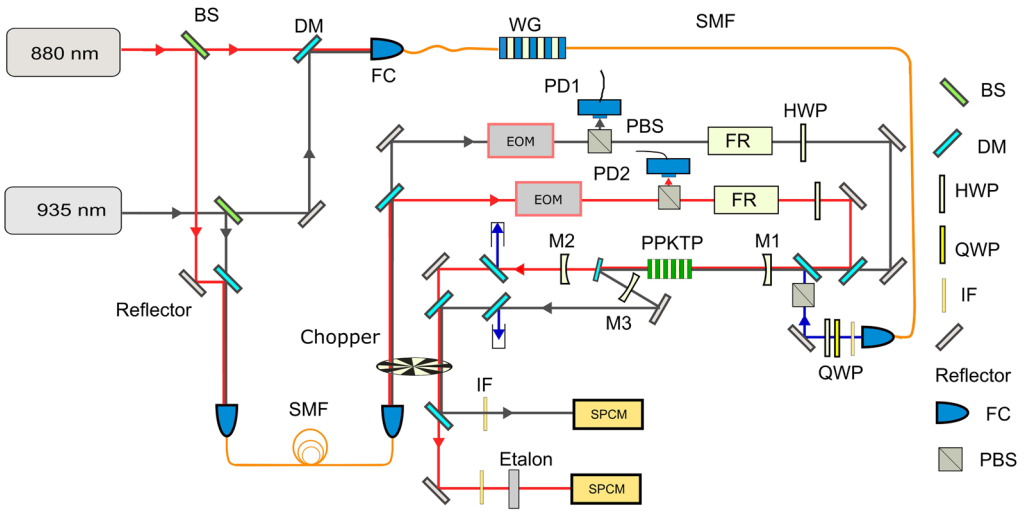

FIG. 1. Experimental setup for narrow-band photon-pair source. BS, beam splitter; HWP, half-wave plate; QWP, quarter-wave plate; PBS, polarization beam splitter; WG, waveguide; EOM, electro-optic modulator; IF, interference filter; FR, Faraday rotator; FC, fiber coupler; PD1, PD2, photodiodes; SMF, single-mode fiber; SPCM, single-photon counting module. The locking beams are frequency modulated at 50 MHz by EOMs to generate the sidebands for the cavity locking. The combination of HWP and FR is to get the reflected laser from the cavity, and the PDs detect the optical signal. The etalon is used to filter out the multimode components.

has a high transmissivity at the wavelength of 880 nm ($T \geq 99.5\%$ for s or p polarization) and a high reflectivity at the wavelength of 935 nm ($R \geq 99.99\%$ for s or p polarization). The incident angle of the DM is approximately 10°, resulting from the stringent demand for the good performance of two wavelengths at the same time. The cavity mirror M1 is high-reflection coated to work as an input coupler ($R \geq 99.8\%$ for 880 and 935 nm), and the cavity mirrors M2, M3 work as the output couplers for 880 and 935 nm, respectively, with a piezoelectric transducer attached on each of them ($R = 97\%$). Thus, the CDC structure is constructed with the help of the inserted dichroic mirror and the input coupler M1. The curvature of all of the cavity mirrors is 10 cm, and the free spectral ranges (FSRs) of the two cavities are approximately 800 MHz. The nonlinear PPKTP crystal is also shared by the two cavities. This design provides a flexible method for overcoming the critical difficulty in matching the central frequencies and bandwidths of the signal and idler photons to different quantum systems. All of the optical elements except the inserted DM are antireflectively coated at 453 nm, such that the pump laser passes the nonlinear PPKTP crystal only once.

To realize the cavity-enhanced SPDC process, the two cavities in our CDC structure are locked to two reference laser beams. Owing to the same traveling direction of the locking beam and SPDC photons, the single-photon counting module (SPCM) may be excessively illuminated. A widely used method is intermittently locking the cavities with a mechanical chopper [31,33]. However, in the nondegenerate case [33], two mechanical choppers are usually needed to block two different locking beams, and a critical phase lock should be achieved between the two choppers, due to the inevitable difference-frequency-generation process in the cavity. In our design, as shown in Fig. 1, two locking beams are combined together, as are the SPDC photon pairs, so that they pass through the chopper and then are separated by the dichroic mirror. These measures ensure that the SPCM will be safe even if the chopper breaks or the electricity shuts off. Moreover, owing to the CDC design, double resonance in one cavity is not required, as it has been in previous reports [31], which will decrease the demand for the accuracy of the temperature control of PPKTP crystal. All of the above improvements make our setup rather robust against external environmental disturbances.

It has been shown that the SPDC photon pairs emitted from the cavity often have a multimode output [27], which decreases the coherence and limits the use of the narrow-band photon pairs in experiments. As a result, we place an etalon filter after the output coupler of the 880-nm cavity (shown in Fig. 1) to eliminate the extra multimode components [31]. The etalon (central wavelength 880 nm, bandwidth 120 MHz, FSR 8.4 GHz) is placed in a temperature-controlled oven with an accuracy of 10 mK to achieve a good filtering effect.

III. RESULTS

To learn more about the generated photon pairs, we collected time-correlated measurements. The specific method is to measure the second-order cross-correlation function $G^{(2)}_{S,I}(\tau)$ between photon pairs [32,33]. The signal and idler photons are separated by a dichroic mirror and fiber coupled into the SPCMs for detection after necessary optical filtering. The time distribution of photon pairs arriving at the detectors is recorded by the time-to-digital converter (Picoquant 400). The measured results of $G^{(2)}_{S,I}(\tau)$ are plotted in Fig. 2. The correlation function is separately fitted on the two sides of the curve referred to as the fitting function $e^{-2\pi\Delta\nu\tau}$, resulting in the signal and idler photon bandwidths being 4 MHz at 935 nm and 5 MHz at 880 nm. The small difference is mainly caused by the different losses of the inserted dichroic mirror at the two wavelengths.

For the purpose of quantum information processing, the high value of the normalized cross-correlation function at zero delay $g^{(2)}_{S,I}(0)$ is crucial. The detailed form of the normalized cross-correlation function is expressed as

$$g^{(2)}_{S,I}(\tau) = \frac{\langle E^{\dagger}_S(t)E^{\dagger}_I(t+\tau)E_I(t+\tau)E_S(t)\rangle}{\langle E^{\dagger}_I(t+\tau)E_I(t+\tau)\rangle\langle E^{\dagger}_S(t)E_S(t)\rangle}, \qquad (1)$$

where $E_{S,I}(\tau)$ indicates the operators of signal and idler fields. It is calculated using the correlation function as the peak value divided by the average count value in the accidental region (in the range from 200 to 250 ns in Fig. 2 [33]). The measured $g^{(2)}_{S,I}(0)$ varying with different input pump power is plotted in Fig. 3, showing a well-fitted inverse-proportion relation [35]. The $g^{(2)}_{S,I}(0)$ is about 88 when the input pump power is 1 mW, much higher than the classical threshold of 2 for two-mode squeezed states. Decreasing the pump power to less than 100 μW, $g^{(2)}_{S,I}(0)$ achieves a high value of approximately 800. All of these values are calculated without subtracting any background

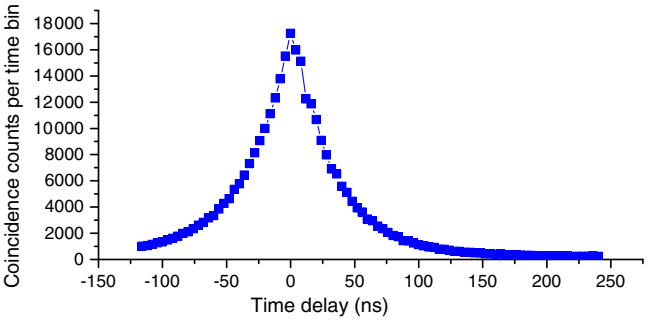

FIG. 2. The correlation function $G^{(2)}_{S,I}(\tau)$ is measured at a pump power of 0.8 mW. The time-bin size is 4 ns and the integration time is 1200 s.

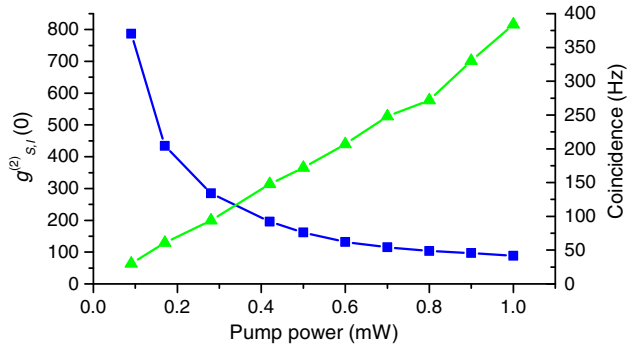

FIG. 3. The measured $g^{(2)}_{S,I}(0)$ versus pump power is plotted on the left axis (blue square). The multimode coincidence rate versus the pump power is plotted on the right axis (green triangle). The coincidence rate is measured by summing all the bins of the coincidence curve divided by the overall measurement time, and subtracting the background counts [30].

counts. The quite-high values of $g^{(2)}_{S,I}(0)$ indicate the good quality of the quantum source and its reliable use in hybrid quantum networks. The coincidence rate as a function of the pump power is also shown in Fig. 3.

The time-resolved measurement $G^{(2)}_{S,I}(\tau)$ of generated cavity-enhanced photon pairs should be a time-domain comblike structure of the curve, because of the interference between different frequency modes [28]. The period of the interference fringe is $t = 1/\mathrm{FSR}$, which is equal to the cavity round-trip time. In our case, as the SPCMs have a resolution time of 350 ps and the cavity round-trip time of 1.25 ns, we obtain imperfect comblike interference fringes, as plotted in Fig. 4. The destructive interference part cannot reach zero, as a result of the small ratio between cavity round-trip time and resolution time. The asymmetry of interference fringes results in the mode difference between the two cavities. Next, an etalon is inserted to filter the unwanted multimodes. Based on the same time-resolved measurement, the comblike structure of the curve nearly disappears, as shown in the inset of Fig. 4. This relatively smooth curve indicates quite a large suppression of multimode photon pairs.

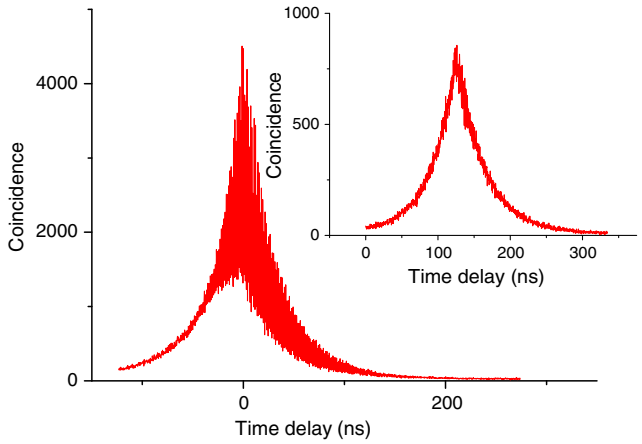

FIG. 4. The measured time-resolved correlation function $G^{(2)}_{S,I}(\tau)$ with the time-bin size of 256 ps. The imperfect comblike interference fringes are due to the low ratio between cavity round-trip time and resolution time. The pump power here is 0.8 mW and the integration time is 3600 s. The inset is measured with the etalon inserted after the 880 nm cavity, showing a good elimination of the multimode components. The pump power here is 1.2 mW and the integration time is 7200 s

To further ensure the single-mode output of the generated photon pairs, we use a Michelson interferometer to measure the coherence of the filtered 880-nm photons [33,37]. The results are shown in Fig. 5. To scan the interference fringes, a reflective mirror in one arm is mounted on a translation stage with a piezoelectric transducer attached for fine tuning. With a 880-nm laser beam fed into the interferometer, a high average interference visibility of approximately 0.99 is observed, showing the good quality of interferometer. Without the etalon filter, the interference fringes show decreasing visibilities with a certain period due to the multimode components. The average interference visibility of the filtered case is 92% in the test region, with a stable trend of high interference visibility when increasing the optical path difference between two arms. The combined measurement of second-order cross correlation and first-order autocorrelation (coherence) provides good evidence that our source can provide the single-mode output.

After the filtering of multimodes, the single-mode photon-pair generation rate is detected at a pump power of 0.9 mW; the rate is approximately 20 photon pairs/s. Considering the bandwidth mentioned above, we can obtain the normalized spectrum brightness of approximately 4.9 photon pairs/(s MHz mW) without any modification. To further improve the spectral brightness, some

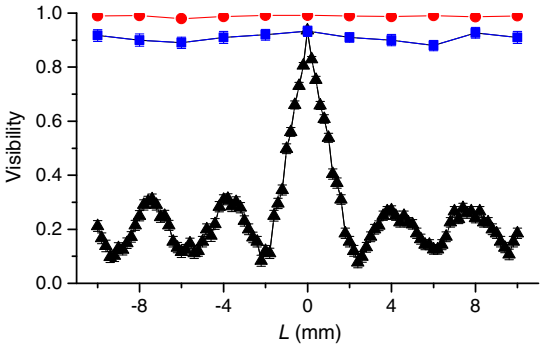

FIG. 5. Measured results of the visibility of the Michelson interferometer versus its optical path difference in three cases, illustrating the coherence of the input light. High-interference visibilities of classical light show the good quality of the interferometer (red circle). Owing to the existence of multimodes, the unfiltered case shows the overall decreasing interference visibilities (black triangle). For the filtered case, the interference visibilities are almost as high as those of the classical case, indicating a good filtering of multimodes (blue square).

available methods are to increase the detection system efficiency (including the losses of the etalon), the finesse of the cavity, and the output proportion of the chopper duty cycle (in our case, $\sim 1/3$).

IV. CONCLUSIONS

In conclusion, we present a CDC strategy to provide nondegenerate narrow-band photon pairs via a cavity-enhanced SPDC process. Based on this strategy, a photon-pair source is experimentally generated with narrow bandwidths of 4 MHz at 935 nm and 5 MHz at 880 nm, which can be applied to link the ion trap node and solid-state quantum memory node in a hybrid quantum network. Because of the special design of the CDC strategy, the central frequencies and bandwidths of both the signal and idler photons in the pair can be individually set to match these two types of nodes very well. This method should be useful for constructing a hybrid quantum network involving nodes of various quantum systems in the future.

ACKNOWLEDGMENTS

We thank Z.-Y. Zhou and Y. Li for their useful discussions and we also thank Z.-Q. Zhou, G.-Y. Xiang, and C.-H. Dong for lending us some experimental devices. This work was supported by the National Natural Science Foundation of China (Grants No. 61327901, No. 61490711, No. 11274289, No. 11325419, No. 61225025, No. 11474268, No. 11374288, No. 11304305, No. 11404319), the National Basic Research Program of China (No. 2011CB921200), the Strategic Priority Research Program (B) of the Chinese Academy of Sciences (Grant No. XDB01030300), the Fundamental Research Funds for the Central Universities (No. WK2470000011, No. WK2470000018).

[1] H. J. Kimble, The quantum Internet, Nature (London) **453**, 1023 (2008).
[2] N. Sangouard, C. Simon, H. de Riedmatten, and N. Gisin, Quantum repeaters based on atomic ensembles and linear optics, Rev. Mod. Phys. **83**, 33 (2011).
[3] S. Ritter, C. Nölleke, C. Hahn, A. Reiserer, A. Neuzner, M. Uphoff, M. Mücke, E. Figueroa, J. Bochmann, and G. Rempe, An elementary quantum network of single atoms in optical cavities, Nature (London) **484**, 195 (2012).
[4] L.-M. Duan and C. Monroe, Quantum networks with trapped ions, Rev. Mod. Phys. **82**, 1209 (2010).
[5] M. Wallquist, K. Hammerer, P. Rabl, M. Lukin, and P. Zoller, Hybrid quantum devices and quantum engineering, Phys. Scr. **T137**, 014001 (2009).
[6] H. M. Meyer, R. Stockill, M. Steiner, C. Le Gall, C. Matthiesen, E. Clarke, A. Ludwig, J. Reichel, M. Atatre, and M. Köhl, Direct Photonic Coupling of a Semiconductor Quantum Dot and a Trapped Ion, Phys. Rev. Lett. **114**, 123001 (2015).
[7] S. Ramelow, A. Fedrizzi, A. Poppe, N. K. Langford, and A. Zeilinger, Polarization-entanglement conserving frequency conversion of photons, Phys. Rev. A **85**, 013845 (2012).
[8] C. Simon, H. de Riedmatten, M. Afzelius, N. Sangouard, H. Zbinden, and N. Gisin, Quantum Repeaters with Photon Pair Sources and Multimode Memories, Phys. Rev. Lett. **98**, 190503 (2007).
[9] R. Blatt and D. Wineland, Entangled states of trapped atomic ions, Nature (London) **453**, 1008 (2008).
[10] J.-M. Cui, Y.-F. Huang, Z. Wang, D.-Y. Cao, J. Wang, W.-M. Lv, Y. Lu, L. Luo, A. del Campo, Y.-J. Han, C.-F. Li, and G.-C. Guo, Supporting Kibble-Zurek mechanism in quantum Ising model through a trapped ion, arXiv: 1505.05734.
[11] T. Monz, P. Schindler, J. T. Barreiro, M. Chwalla, D. Nigg, W. A. Coish, M. Harlander, W. Hänsel, M. Hennrich, and R. Blatt, 14-Qubit Entanglement: Creation and Coherence, Phys. Rev. Lett. **106**, 130506 (2011).
[12] J. W. Britton, B. C. Sawyer, A. C. Keith, C.-C. J. Wang, J. K. Freericks, H. Uys, M. J. Biercuk, and J. J. Bollinger, Engineered two-dimensional Ising interactions in a trapped-ion quantum simulator with hundreds of spins, Nature (London) **484**, 489 (2012).
[13] H. Häffner, C. F. Roos, and R. Blatt, Quantum computing with trapped ions, Phys. Rep. **469**, 155 (2008).
[14] A. Stute, B. Casabone, P. Schindler, T. Monz, P. O. Schmidt, B. Brandstätter, T. E. Northup, and R. Blatt, Tunable ion-photon entanglement in an optical cavity, Nature (London) **485**, 482 (2012).
[15] D. L. Moehring, P. Maunz, S. Olmschenk, K. C. Younge, D. N. Matsukevich, L.-M. Duan, and C. Monroe, Entanglement of single-atom quantum bits at a distance, Nature (London) **449**, 68 (2007).
[16] N. Piro, F. Rohde, C. Schuck, M. Almendros, J. Huwer, J. Ghosh, A. Haase, M. Hennrich, F. Dubin, and J. Eschner, Heralded single-photon absorption by a single atom, Nat. Phys. **7**, 17 (2011).
[17] M. Schug, J. Huwer, C. Kurz, P. Müller, and J. Eschner, Heralded Photonic Interaction between Distant Single Ions, Phys. Rev. Lett. **110**, 213603 (2013).
[18] H. de Riedmatten, M. Afzelius, M. U. Staudt, C. Simon, and N. Gisin, A solid-state light-matter interface at the single-photon level, Nature (London) **456**, 773 (2008).
[19] D. Rieländer, K. Kutluer, P. Ledingham, M. Gündoğan, J. Fekete, M. Mazzera, and H. de Riedmatten, Quantum Storage of Heralded Single Photons in a Praseodymium-Doped Crystal, Phys. Rev. Lett. **112**, 040504 (2014).
[20] G. Heinze, C. Hubrich, and T. Halfmann, Stopped Light and Image Storage by Electromagnetically Induced Transparency up to the Regime of One Minute, Phys. Rev. Lett. **111**, 033601 (2013).
[21] Z.-Q. Zhou, W.-B. Lin, M. Yang, C.-F. Li, and G.-C. Guo, Realization of Reliable Solid-State Quantum Memory for Photonic Polarization Qubit, Phys. Rev. Lett. **108**, 190505 (2012).
[22] Z.-Q. Zhou, Y.-L. Hua, X. Liu, G. Chen, J.-S. Xu, Y.-J. Han, C.-F. Li, and G.-C. Guo, Quantum Storage of Three-Dimensional Orbital-Angular-Momentum Entanglement in a Crystal, Phys. Rev. Lett. **115**, 070502 (2015).

[23] E. Saglamyurek, J. Jin, V. B. Verma, M. D. Shaw, F. Marsili, S. Woo Nam, D. Oblak, and W. Tittel, Quantum storage of entangled telecom-wavelength photons in an erbium-doped optical fibre, Nat. Photonics **9**, 83 (2015).

[24] F. Bussières, C. Clausen, A. Tiranov, B. Korzh, V. B. Verma, S. Woo Nam, F. Marsili, A. Ferrier, P. Goldner, H. Herrmann, C. Silberhorn, W. Sohler, M. Afzelius, and N. Gisin, Quantum teleportation from a telecom-wavelength photon to a solid-state quantum memory, Nat. Photonics **8**, 775 (2014).

[25] M. Zhong, M. P. Hedges, R. L. Ahlefeldt, J. G. Bartholomew, S. E. Beavan, S. M. Wittig, J. J. Longdell, and M. J. Sellars, Optically addressable nuclear spins in a solid with a six-hour coherence time, Nature (London) **517**, 177 (2015).

[26] J. K. Thompson, J. Simon, H. Loh, and V. Vuletic, A high-brightness source of narrowband, identical-photon pairs, Science **313**, 74 (2006).

[27] Z. Y. Ou and Y. J. Lu, Cavity Enhanced Spontaneous Parametric Down-Conversion for the Prolongation of Correlation Time between Conjugate Photons, Phys. Rev. Lett. **83**, 2556 (1999).

[28] H. Wang, T. Horikiri, and T. Kobayashi, Polarization-entangled mode-locked photons from cavity-enhanced spontaneous parametric down-conversion, Phys. Rev. A **70**, 043804 (2004).

[29] C. E. Kuklewicz, F. N. C. Wong, and J. H. Shapiro, Time-Bin-Modulated Biphotons from Cavity-Enhanced Down-Conversion, Phys. Rev. Lett. **97**, 223601 (2006).

[30] Z.-Y. Zhou, D.-S. Ding, Y. Li, F.-Y. Wang, and B.-S. Shi, Cavity-enhanced bright photon pairs at telecom wavelengths with a triple-resonance configuration, J. Opt. Soc. Am. B **31**, A1 (2014).

[31] X.-H. Bao, Y. Qian, J. Yang, H. Zhang, Z.-B. Chen,T. Yang, and J.-W. Pan, Generation of Narrow-Band Polarization-Entangled Photon Pairs for Atomic Quantum Memories, Phys. Rev. Lett. **101**, 190501 (2008).

[32] F. Wolfgramm, Y. A. de Icaza Astiz, F. A. Beduini, A. Cerè, and M. W. Mitchell, Atom-Resonant Heralded Single Photons by Interaction-Free Measurement, Phys. Rev. Lett. **106**, 053602 (2011).

[33] J. Fekete, D. Rieländer, M. Cristiani, and H. de Riedmatten, Ultranarrow-Band Photon-Pair Source Compatible with Solid State Quantum Memories and Telecommunication Networks, Phys. Rev. Lett. **110**, 220502 (2013).

[34] M. Förtsch, J. U. Fürst, C. Wittmann, D. Strekalov, A. Aiello, M. V. Chekhova, C. Silberhorn, G. Leuchs, and C. Marquard, A versatile source of single photons for quantum information processing, Nat. Commun. **4**, 1818 (2013).

[35] K.-H. Luo, H. Herrmann, S. Krapick, R. Ricken, V. Quiring, H. Suche, W. Sohler, and C. Silberhorn, Two-color narrow-band photon pair source with high brightness based on clustering in a monolithic waveguide resonator, arXiv: 1306.1756.

[36] E. D. Black, An introduction to Pound-Drever-Hall laser frequency stabilization, Am. J. Phys. **69**, 79 (2001).

[37] F.-Y. Wang, B.-S. Shi, C. Zhai, and G.-C. Guo, Experimental measuring of the coherence length of a single photon generated via a degenerated optical parametric oscillator far below threshold, J. Mod. Opt. **57**, 330 (2010).